AGU ADVANCING EARTH AND SPACE SCIENCE

Geophysical Research Letters®

RESEARCH LETTER
10.1029/2021GL097014

Key Points:

- Meteorite paleomagnetism and hybrid modeling imply that asteroids may form magnetospheres and trap charged particles
- Planning of missions to asteroids requires assessing trapped particle energies, but existing models are not valid for such magnetospheres
- A new nonadiabatic trapping criterion shows that asteroids should not have hazardous particle radiation belts

Supporting Information:

Supporting Information may be found in the online version of this article.

Correspondence to:

R. Oran,
roran@mit.edu

Citation:

Oran, R., Weiss, B. P., De Soria Santacruz-Pich, M., Jun, I., Lawrence, D. J., Polanskey, C. A., et al. (2022). Maximum energies of trapped particles around magnetized planets and small bodies. *Geophysical Research Letters*, *49*, e2021GL097014. https://doi.org/10.1029/2021GL097014

Received 18 NOV 2021
Accepted 15 APR 2022

Author Contributions:

Conceptualization: Benjamin P. Weiss, Insoo Jun, Carol A. Polanskey, Carol A. Raymond, Linda T. Elkins-Tanton
Formal analysis: Insoo Jun, Christopher T. Russell, Yuri Y. Shprits
Funding acquisition: Carol A. Polanskey, Linda T. Elkins-Tanton
Investigation: Benjamin P. Weiss, Maria De Soria Santacruz-Pich, David J. Lawrence, Carol A. Polanskey, J. Martin Ratliff, Carol A. Raymond, Jodie B. Ream, Christopher T. Russell, Yuri

Maximum Energies of Trapped Particles Around Magnetized Planets and Small Bodies

Rona Oran[1], Benjamin P. Weiss[1], Maria De Soria Santacruz-Pich[2], Insoo Jun[2], David J. Lawrence[3], Carol A. Polanskey[2], J. Martin Ratliff[2], Carol A. Raymond[2], Jodie B. Ream[1], Christopher T. Russell[4], Yuri Y. Shprits[5,6,7], Maria T. Zuber[1], and Linda T. Elkins-Tanton[8]

[1]Department of Earth, Atmospheric, and Planetary Sciences, Massachusetts Institute of Technology, Cambridge, MA, USA, [2]Jet Propulsion Laboratory, California Institute of Technology, Pasadena, CA, USA, [3]The Johns Hopkins University Applied Physics Laboratory, Laurel, MD, USA, [4]Institute of Geophysics and Planetary Physics, University of California, Los Angeles, CA, USA, [5]Helmholtz Centre Potsdam, GFZ German Research Centre for Geosciences, Potsdam, Germany, [6]Department of Earth, Planetary, and Space Sciences, University of California, Los Angeles, CA, USA, [7]Institute of Physics and Astronomy, University of Potsdam, Potsdam, Germany, [8]School of Earth and Space Exploration, Arizona State University, Tempe, AZ, USA

Abstract Energetic charged particles trapped in planetary radiation belts are hazardous to spacecraft. Planned missions to iron-rich asteroids with possible strong remanent magnetic fields require an assessment of trapped particles energies. Using laboratory measurements of iron meteorites, we estimate the largest possible asteroid magnetic moment. Although weak compared to moments of planetary dynamos, the small body size may yield strong surface fields. We use hybrid simulations to confirm the formation of a magnetosphere with an extended quasi-dipolar region. However, the short length scale of the field implies that energetic particle motion would be nonadiabatic, making existing radiation belt theories not applicable. Our idealized particle simulations demonstrate that chaotic motions lead to particle loss at lower energies than those predicted by adiabatic theory, which may explain the energies of transiently trapped particles observed at Mercury, Ganymede, and Earth. However, even the most magnetized asteroids are unlikely to stably trap hazardous particles.

Plain Language Summary Radiation belts are regions in space filled with energetic charged particles trapped by a planetary magnetic field. To date, radiation belts were found around Earth, Jupiter, Saturn, Uranus, and Neptune. Understanding radiation belts is important because they can be hazardous to spacecraft. In addition, their emission, if detected remotely, can reveal a planet's magnetic field. The future exploration of asteroids and exoplanets may lead to the discovery of more magnetized bodies, including the upcoming NASA mission to asteroid (16) Psyche, the largest known metal-rich planetary object. Existing radiation belt theory was developed for known radiation belts surrounding the large, highly magnetized planets in the solar system. However, the nature of particle trapping should differ for small bodies like asteroids. We examine these differences to provide predictive tools for the existence of belts that can be applied to any kind of magnetosphere. We find a class of bodies that can sustain belt-like structures but where particle trajectories are chaotic, preventing prolonged stable trapping and associated energization. We show that Mercury and Ganymede's transient trapping is consistent with our predictions. Finally, we show that although asteroids may stably trap low-energy protons and electrons, even the most strongly magnetized metallic asteroids cannot form belts that pose a risk to typical spacecraft hardware.

1. Introduction

Radiation belts consist predominantly of energetic charged particles trapped in a planetary magnetic field. They are of interest due to their role in magnetospheric dynamics and in aiding the detection of planetary fields (Roussos et al., 2019), and the hazard they pose to spacecraft hardware (Baker et al., 2018). Jupiter's and Earth's radiation belts were first detected at the beginning of the space age (Drake & Hvatum, 1959; Van Allen et al., 1958) and analogous belts have since been found around Saturn, Uranus, and Neptune, all exhibiting long-term trapping of particles with energies up to 1 MeV and maybe 2 GeV (Adriani et al., 2015; Mauk & Fox, 2010; Roussos et al., 2018). Around smaller bodies like Mercury and Ganymede, trapped particles of $\sim 10^2$ keV were detected but were likely quickly lost (Eviatar et al., 2000; Ho et al., 2011; Lawrence et al., 2015; Liuzzo et al., 2020; Poppe

Y. Shprits, Maria T. Zuber, Linda T. Elkins-Tanton
Methodology: Maria De Soria Santacruz-Pich, Insoo Jun, David J. Lawrence, J. Martin Ratliff, Christopher T. Russell, Yuri Y. Shprits, Linda T. Elkins-Tanton
Project Administration: Benjamin P. Weiss, Maria De Soria Santacruz-Pich, Carol A. Polanskey, Linda T. Elkins-Tanton
Resources: Benjamin P. Weiss, Carol A. Polanskey, Linda T. Elkins-Tanton
Supervision: Benjamin P. Weiss, Carol A. Polanskey, Linda T. Elkins-Tanton
Validation: Insoo Jun, J. Martin Ratliff, Carol A. Raymond, Christopher T. Russell, Yuri Y. Shprits, Maria T. Zuber, Linda T. Elkins-Tanton
Writing – review & editing: Benjamin P. Weiss, Maria De Soria Santacruz-Pich, Insoo Jun, David J. Lawrence, Carol A. Polanskey, J. Martin Ratliff, Carol A. Raymond, Jodie B. Ream, Yuri Y. Shprits, Maria T. Zuber, Linda T. Elkins-Tanton

et al., 2018; Williams, 2001, 2004) (Figure 1a and Table S1 in Supporting Information S1). Upcoming missions to potentially magnetized asteroids present yet another, largely unexplored regime. To prepare for this, here we estimate whether small bodies can trap particles and up to what energies, assess the potential hazard to spacecraft, and anticipate science opportunities such as remote detection of planeary magnetism, and studying magnetospheric dynamics.

To date, asteroids explored by spacecraft are thought to be largely rocky and presented no clear evidence of remanent magnetization (Blanco-Cano et al., 2003; Kivelson et al., 1995; Richter et al., 2001; Russell et al., 2018; Scheinberg et al., 2017; Wang et al., 1995). Nevertheless, remanent magnetization has been identified in a variety of meteorites (Terho et al., 1993), suggestive of past dynamo action in their asteroidal parent bodies (Harrison et al., 2017; Scheinberg et al., 2017; Weiss et al., 2010). The upcoming Psyche mission will explore asteroid (16) Psyche (Elkins-Tanton et al., 2020), the largest known iron-rich solar system body (with an effective radius, $R_p = 113$ km; Shepard et al., 2017). Because iron-rich asteroids may carry remanent magnetization similar to that found in iron meteorites, they may have high surface magnetic fields (Table S1 in Supporting Information S1) that may form a magnetosphere and trap particles.

For a typical spacecraft with >2.5 mm of aluminum-equivalent shielding, only energies of >1 MeV for electrons and >20 MeV for protons may pose a risk (Berger et al., 2017). The locations around a dipole field that allow permanent trapping in belt-like structures were first determined analytically under the adiabatic approximation by Störmer (1955). Störmer's method is widely used and was extended to nondipolar planetary fields (Lemaire et al., 2003; Tsareva, 2019). It predicts trapping up to energies of ∼1–10 GeV around the Earth (Schulz & Lanzerotti, 1974), Saturn, and Jupiter (Birmingham, 1982) and indeed, such trapped populations were detected at those planets (Reeves et al., 2016). However, if applied to Mercury, Störmer's method would erroneously predict trapping of >10 MeV electrons, two orders of magnitude higher than the observed maximal energies of transiently trapped electrons (Ho et al., 2011; Lawrence et al., 2015). While the high day-night asymmetry of Mercury's magnetosphere (Slavin et al., 2007) might explain this discrepancy, it is likely that violation of adiabatic invariance due to the small scale of Mercury's field is at least partly responsible. Störmer method is likely not valid for the still smaller magnetospheres that may be formed by asteroids.

Building on decades of spacecraft in situ measurements, complex radiation belt models for Earth have been developed, incorporating high order particle acceleration and loss mechanisms (Baker et al., 2018). However, these too rely on the assumption of underlying adiabatic motion (Horne et al., 2005) and in any case are not readily applicable for bodies of arbitrary size, planetary rotation rate, and distance from the Sun. Furthermore, Earth's atmosphere is an important source of energetic particles injected into the belts, but such sources are negligible for iron-rich airless bodies (Lawrence et al., 2016). Due to this gap in theory, here we use verified theoretical and computational tools (Supporting Information S1), apply them to the novel scenario of trapping in hypothetical asteroid magnetospheres, and generalize the results to any body size and dipole moment. First, we use hybrid simulations and iron meteorite measurements to establish that magnetospheres could indeed exist around large iron-rich asteroids. To avoid the uncertainty of whether acceleration mechanisms known for the terrestrial magnetosphere would be present, we determine the maximum energies at which particles can be stably trapped regardless of how and whether such particles were created. We consider the limits of adiabatic motion by tracing single particle motion and identify chaotic pitch angle scattering due to high field curvature as a critical limiting factor for trapping even in a steady state dipole field. While nonadiabatic scattering was previously studied in nondipolar regions of planetary magnetospheres (Anderson et al., 1997; Selesnick et al., 2001), it was not applied to study the location and energies of radiation belts, which reside in quasi-dipolar regions and are predominantly adiabatic for large magnetospheres. Finally, we obtain a nonadiabatic trapping criterion that can serve planned and future exploration for any small body, and validate it against relevant observations at Ganymede, Mercury, and Earth.

2. The Possibility of Asteroid Magnetospheres

To allow trapping of particles of a given energy, an asteroidal magnetic field must first be sufficiently strong to form a magnetospheric cavity in the solar wind that is larger than the particles' gyroradii, r_g, so that particles can gyrate without intersecting the surface or the magnetopause. An upper limit for asteroid fields can be inferred from laboratory measurements of the specific magnetization of iron meteorites, some of the most magnetic meteorites known. These mostly fall in the range of 10^{-4} to 10^{-2} Am^2 kg^{-1} (Pesonen et al., 1992; Terho et al., 1993). The

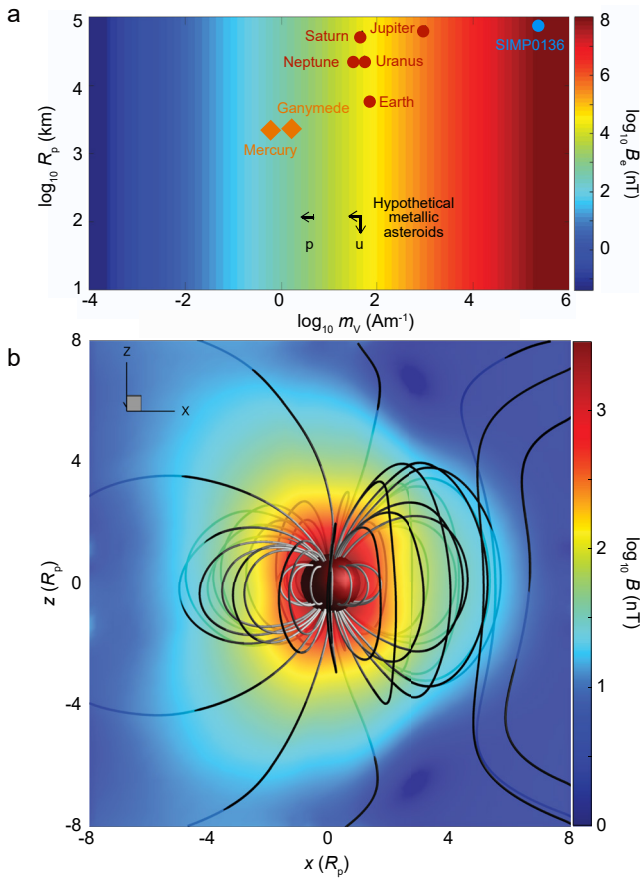

Figure 1. (a) Equatorial surface magnetic field for known and hypothetical magnetized bodies organized by radius, R_p, and magnetic moment per unit volume, m_V (Table S1 in Supporting Information S1). Circles denote bodies with confirmed belts (red circles for solar system bodies, blue circle for the magnetized exoplanet/brown dwarf SIMP0136). Orange diamonds denote bodies with transient trapping of <1 MeV electrons. Black arrows mark the upper limits of asteroid magnetization: *u* marks the extreme case of a uniformly magnetized asteroid and *p* marks the strongest feasible Psychean dipole moment. (b) 3D hybrid simulation of the maximum feasible Psychean field, marked by *p* in (a). The dipole axis points in the $+z$ direction, the solar wind flows in the $-x$ direction, and the interplanetary magnetic field points in the $+z$ direction. The color contours show the field magnitude in the x-z plane and on the surface; closed field lines show drift shells with an equatorial field of 330 nT (innermost shell), 31 nT, and 18 nT (outermost shell). Representative open and solar wind field lines are also shown.

maximum hypothetical asteroid field in the solar system would be obtained for the largest iron-rich asteroid, Psyche (mass of $2.72 \pm 0.75 \times 10^{19}$ kg, Carry, 2012), assuming it was uniformly magnetized at the high end of this magnetization range. This yields a dipole moment, $M_d = 2.7 \times 10^{17}$ Am^2, and an equatorial surface field, B_e = 19,000 nT. Although this predicted field is comparable to that of the Earth, the predicted moment is five orders of magnitude less than that of the Earth (Table S1 in Supporting Information S1 and Figure 1a). These values are extreme upper limits given that asteroids are almost certainly nonuniformly magnetized.

The leading hypothesis for Psyche's origin is that it is a mantle-stripped metallic core from a differentiated body (Elkins-Tanton et al., 2020). Such a bare core could have potentially generated a dynamo field lasting for >7 million years (Ma) (Neufeld et al., 2019). Because such a dynamo is expected to be highly multipolar and time-variable (Neufeld et al., 2019), different parts of the body would record different field directions as it cooled. Subsequent impacts may have further changed the magnetization by either remagnetizing or displacing materials. To estimate the maximum dipole moment of such a nonuniformly magnetized body, we assume the outer ~40% of the radius of the body is a magnetized crust, as indicated by a recent dynamo and thermal evolution model of Psyche-like bodies (Neufeld et al., 2019). Crustal fields on Mars, the Moon, and the Earth were shown to be consistent with those of a shell or sphere packed with randomly oriented dipoles sometimes laterally correlated (Voorhies, 1998, 2008; Voorhies et al., 2002; Wieczorek, 2018). We take the limiting case that the magnetization is correlated over a spatial scale equal to 40% of the radius of the body, such that the body is made of closely packed spherical domains of 40 km diameter that are uniformly magnetized in random directions. The number of spheres closely packed into a body of a given volume is given by well-known relationships (Hales, 2005). For 40 km spheres fitted into a 113 km sphere this corresponds to N = 120–130 spherical domains. The dipole moment of such a distribution would be ≈0.1 of the moment of a uniformly magnetized assemblage (Heslop, 2007), yielding $M_d = 2.7 \times 10^{16}$ Am^2, and B_e = 1,900 nT.

The above represents the maximum feasible asteroid field (most asteroids are rocky and consist of weakly magnetic minerals and may lack remanent magnetization altogether). We can estimate the size of the magnetosphere created by such a limiting body by calculating the dayside magnetopause distance, R_{MP}, given the solar wind properties in the asteroid belt. We find (Section S1 in Supporting Information S1) that $R_{MP} \approx 4.7$–$5.4 R_p \approx 530$ – 610 km. In comparison, the solar wind proton and electron thermal gyroradii at the asteroid belt are ~150 km and ~5 km, respectively (Section S1 in Supporting Information S1), implying that the field is large enough to deflect these particles and thus form a magnetospheric cavity.

Radiation belts form in the inner regions of planetary magnetospheres where the field is quasi-dipolar and trapped particle motion can be stably sustained. At larger distances, the interaction with surrounding magnetized plasmas distorts the field and may prevent particles from completing full drift motions (Klida & Fritz, 2009; Schulz & Lanzerotti, 1974; Walsh et al., 2013). To estimate the extent of the inner quasi-dipolar region for our limiting case of an asteroid magnetosphere, we simulated the interaction of a Psyche-sized body with $M_d = 2.7 \times 10^{16}$ Am^2 with the solar wind. Because the proton gyroradius is comparable to R_p, we used a hybrid particle-fluid code, HYB, which treats electrons as a fluid and protons as particles. HYB has been used to simulate the interaction of the wind with various planets, moons, and asteroids (Kallio & Janhunen, 2003). To adapt the model to a metallic body, we set the body's resistivity to zero, consistent with the fact that iron-nickel alloys are highly conducting (Fert & Campbell, 1976). This constitutes the first three-dimensional (3D) hybrid simulation of a

perfectly conducting and magnetized asteroid (Section S4 in Supporting Information S1). In previously published 3D hybrid models of a Psyche-sized magnetized asteroid (Fatemi & Poppe, 2018) the body had a conductivity of 10^{-7} S m^{-1} (similar to the lunar crust). The currents induced within a conducting body should have a minimal effect on the steady state magnetosphere of a body with high magnetic moment but may become important for weaker magnetization or for a realistically time-variable solar wind.

The resulting 3D magnetic field topology is shown in Figure 1b, confirming that a Psyche-like asteroid can form a magnetosphere with a dayside magnetopause distance of ~6 R_p (consistent with the above) and with a dipole-like inner region extending up to ~3 R_p. The maximum feasible dipole moment presented here is ~3–10 times larger than the dipole moments assumed in Fatemi and Poppe (2018), and R_{MP} is ~1 R_p larger than the largest magnetosphere simulated in Fatemi and Poppe (2018). Figure 1b represents the largest feasible present-day asteroid magnetosphere in the solar system.

The 3D hybrid simulations presented here and in Fatemi and Poppe (2018) cannot account for the formation of radiation belts; the simulations' high computational cost limits the simulated time to a few tens of seconds (Section S4 in Supporting Information S1), sufficient to obtain a steady state global magnetosphere, but insufficient time for electrons to accelerate from typical solar wind energies (thermal and bulk flow) of <10 eV to hazardous (>1 MeV) levels. Although Fatemi and Poppe (2018) reported a density enhancement on the night side inner magnetosphere, it is unlikely to be made of trapped energetic particles due to the short simulation time (note that the energies were not reported therein). Moreover, energetic protons would be lost already for energies >10 keV, as we show in Section 4.

3. Violation of Adiabatic Motion

Under the adiabatic approximation, partilce trajectories in quasi-dipolar magnetic fields are fully described by the three adiabatic invariants, J_i (i = 1,2,3), which are integrals of motion taken over three generalized coordinates: Q_1, the path length along the gyration motion, Q_2, the path length along the field line due to bounce motions between the mirror points, and Q_3, the angle spanned by the longitudinal drift motion (Northrop, 1963; Stern, 1971). Particles conserving all three J_i's are permanently trapped in toroidal shells (Figures 2a–2c). The locations of these shells depend on the value of J_3 through the dimensionless parameter $\gamma_3 \equiv -(1/2)\sqrt{r_{eq}/r_g} \propto J_3$ (Störmer, 1955), where r_{eq} is the radial distance where the field line intersects the magnetic equatorial plane. Permanent trapping can be achieved for $\gamma_3 < -1$ (Gombosi, 2004; Lemaire et al., 2003; Störmer, 1955). This can be rewritten as a condition on the gyroradius:

$$r_g < \frac{r_{eq}}{4} = \frac{LR_p}{4} \tag{1}$$

where $L = r_{eq}/R_p$. Equation 1 defines Störmer's trapping regions, or the maximum allowed gyroradius of trapped particles at a given L shell in a dipole field. However, Störmer's method is only valid for particles conserving all three adiabatic invariants, which in turn requires that the three motions occur on disparate timescales, such that $\omega_g \gg \omega_b \gg \omega_d$, where ω_g, ω_b, and ω_d are the gyration, bounce, and drift frequencies, respectively. For an Earth-strength dipole field, these frequencies are separated by three or more orders of magnitude up to very high energies and large L values [Figure 2d, following Schulz and Lanzerotti (1974)]. In contrast, for asteroidal fields, the three frequencies are much closer together for most locations and energies even in the extreme case of uniform and maximal remanent magnetization ($M_d = 2.7 \times 10^{17}$ Am^2, Figure 2e). Because the particle is an oscillator with three degrees of freedom, when any pair of frequencies are comparable, the corresponding motions are no longer independent but would resonantly interact, leading to an exchange of energy between them (Chirikov, 1979). In particular, particles with comparable gyration and bounce periods would suffer exchange of kinetic energy between the velocity components perpendicular and parallel to the magnetic field, $\mathbf{v}_\parallel$ and $\mathbf{v}_\perp$, respectively. This exchange would manifest as changes in the particle pitch angle, α. For modest nonadiabaticity, the variations in the J_i's are periodic and bounded, but as nonadiabaticity increases, the variations become chaotic (Chirikov, 1979). This would amount to pitch angle scattering that would cause particles to enter the loss cone (Serebrennikov et al., 2001). This nonadiabatic effect limits trapped particle energies, as observed in plasma confinement devices (Uckan, 1982).

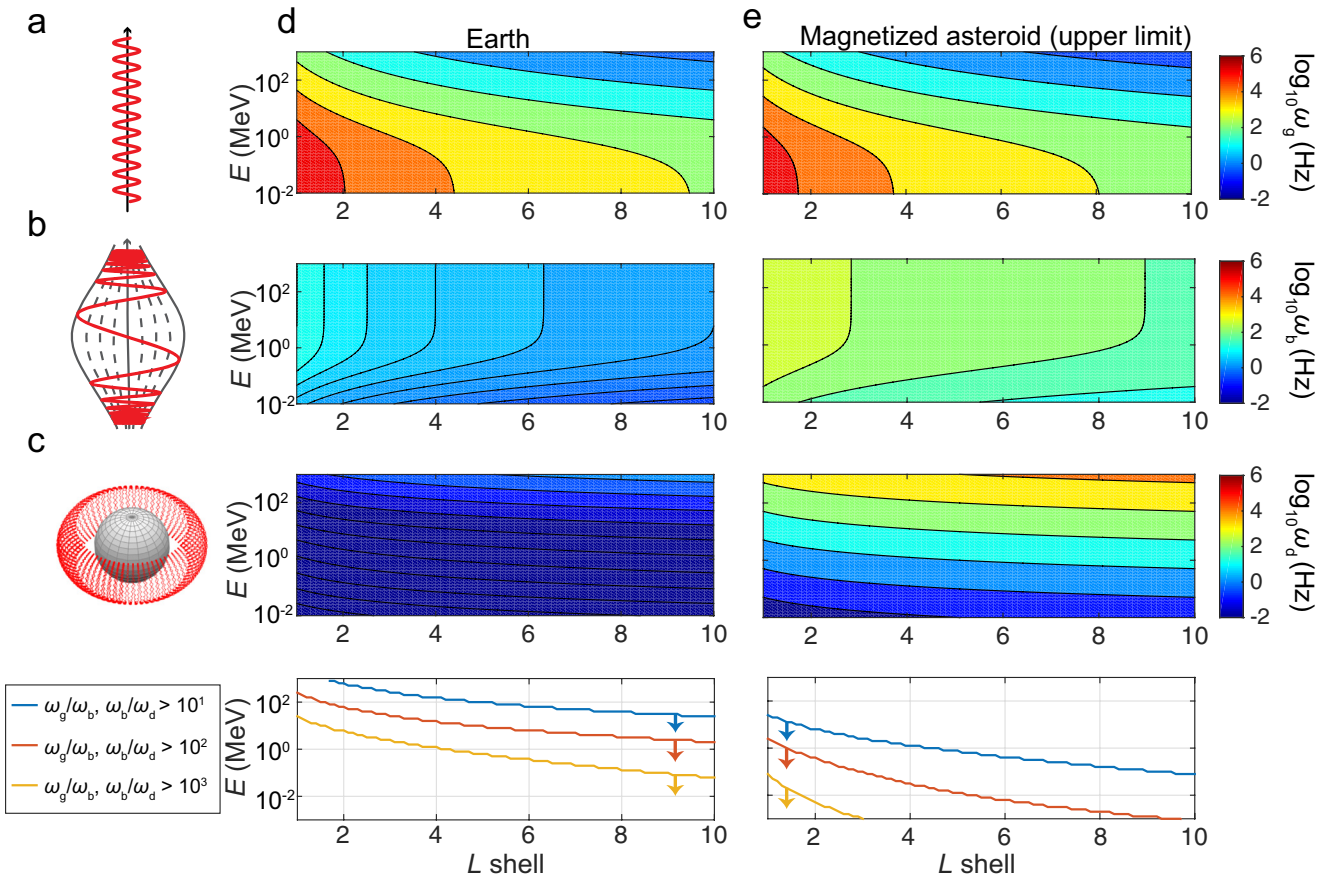

Figure 2. Periodic particle motions in the magnetospheres of Earth and an asteroid. (a) Gyration motion (red) in a uniform magnetic field (black arrow). (b) Bounce motion (red) in a magnetic bottle configuration (gray curves). (c) Particle gyrating, bouncing, and drifting azimuthally (red) around a body (gray sphere) with a dipole field. (d, e) Frequencies of motion as a function of particle energy, E, and L shell assuming a dipole magnetic field for Earth (d) and for the worst-case uniformly magnetized asteroid with the maximal magnetization (e). The panels (top to bottom) show the gyration, bounce, and drift frequencies, and curves indicating where the frequencies are separated by one, two, and three orders of magnitude.

To estimate these maximal energies, we must quantify the level of nonadiabaticity in a quasi-dipolar magnetic field. Several measures have been developed for distorted field lines at Earth (Anderson et al., 1997; Lee et al., 2006; Sergeev et al., 1983; Young et al., 2008), perhaps the simplest of which is the adiabaticity parameter, $\varepsilon \equiv r_g/R_c$, where R_c is the field line radius of curvature (Anderson et al., 1997). In the limit of $\varepsilon \ll 1$, the motion is adiabatic and $\varepsilon \propto \omega_b/\omega_g$. For $\varepsilon > 1$, the motion is nonadiabatic and even chaotic. At this limit ω_g, ω_b, and ω_d are not well-defined (in fact, the assumptions underlying Figure 2e are no longer valid).

We next derive an expression for ε for a dipole field, assuming it is a bounding case for long-term trapping in drift shells (an assumption we further justify below). The maximal ε that a particle would experience during the bounce motion would occur at the magnetic equatorial plane, where r_g is highest and R_c is lowest, having a value of $R_c = LR_p/3$ (Section S2 in Supporting Information S1). Nonadiabatic motion therefore would occur for:

$$r_g > \frac{\varepsilon_{th} L R_p}{3} \tag{2}$$

where the threshold value for the adiabaticity parameter, ε_{th}, is yet to be determined. Before we do so, we make two observations. First, despite the mathematical similarity between Equation 2 and Störmer's criterion (Equation 1), the two describe fundamentally different regimes and loss mechanisms: Equation 1 assumes J_1 and J_2 are conserved and predicts particle loss due to the violation of J_3 due to particles crossing many L shells. In contrast, Equation 2 marks the violation of J_1 and J_2 due to pitch angle scattering and subsequent particle escape through

the loss cone. Second, Equation 2 highlights how trapping is affected by the body size and moment. We can recast ε as:

$$\varepsilon = \frac{r_g}{R_c} = \frac{\gamma m v_\perp}{q} \frac{3L^2}{R_p B_e} \propto \frac{R_p^2}{M_d} \tag{3}$$

where m and q are the particle mass and charge, respectively, and γ is the relativistic Lorentz factor. The last term, showing that $\varepsilon \propto R_p^2$, highlights the fact that smaller bodies have stronger surface fields for the same moment. On the other hand, because $\varepsilon \sim 1/R_p B_e$, even if a Psyche-sized body had a surface field as strong as the Earth's, the limiting gyroradius would be ~60 times smaller than the limiting gyroradius at the same L shell at Earth, meaning the limiting energy would be smaller as well.

We next determine the value of ε at which the transition to chaotic motion occurs. For disturbed (nondipolar) magnetic configurations at Earth, values between $\varepsilon \sim 0.1$–0.3 were derived (Anderson et al., 1997; Lee et al., 2006; Sergeev et al., 1983; Young et al., 2008). Birmingham (1982) set the limiting value for adiabaticity at $\varepsilon = 1$ for Saturn and Jupiter [note that the expression for ε in Birmingham (1982) reduces to the expression we derived in Equation 3 when the former is applied to a pure dipole field]. This limit gives maximum energies well above the energies found in these magnetospheres (Figure 4 therein), implying that the actual limiting value is likely lower. Furthermore, calculating ε for the same range of bodies included in Figure 1a (corresponding to 1 MeV electrons and protons injected at $L = 2$ with $\alpha_{eq} = 90°$) (Figures 3a and 3b) shows that all bodies with known radiation belts are to the right of the $\varepsilon = 0.01$ curves for both electrons and protons, while Mercury and Ganymede, which transiently trap electrons but not protons, fall within the $0.01 < \varepsilon < 0.15$ range for 1 MeV electrons and in the nonadiabatic range ($\varepsilon \approx 1$) for 1 MeV protons. All conceivable asteroids fall well above $\varepsilon = 1$ for protons but the most magnetized among them may reach $\varepsilon \approx 0.26$ for 1 MeV electrons. While this evidence from known trapped populations suggests the transition to chaos would occur around $0.01 < \varepsilon < 0.15$ and above, further analysis is required to obtain a generalized criterion for any small body and predict risk from asteroid magnetospheres.

4. Tracing the Transition to Chaos With Particle Simulations

We next examine under what conditions particle trajectories become chaotic by explicitly solving the equation of motion in a dipole field. This is an optimal case for trapped adiabatic motion because loss is then only triggered by the length scale of the field. Any perturbations and distortions of the field present in a realistic magnetosphere are unlikely to make the motion more adiabatic. While the static dipole approximation is not suitable for examining particle energization, it is the most appropriate for examining whether such particles, if created or injected, could be trapped for arbitrary M_d and R_p. In particular, it is a good approximation of the quasi-dipolar fields where belts reside. We trace the trajectories using an existing fourth order Runge-Kutta solver and apply it to the relativistic Lorentz force (Section S5.1 in Supporting Information S1). Chaotic trajectories are highly sensitive to the initial conditions and therefore also to roundoff errors when they are simulated numerically (Li & Liao, 2018) and the exact trajectory cannot be reliably simulated on standard computers with double-precision floating point representation (Li & Liao, 2018). We therefore do not attempt to capture the exact time of loss (or particle lifetimes) but rather examine whether the particle exhibits pitch angle variations and sensitivity to initial conditions that imply a chaotic regime (Section S5.3 in Supporting Information S1)

Since protons are chaotic for all conceivable asteroids (Figure 3a), we focus on electron motion. We simulated electrons with energy $E = 1$ MeV around a body with $R_p = 113$ km, injected at the equator at $L = 2$. The initial speeds, $v_\parallel$ and $v_\perp$ are in the radial and polar directions, respectively, depending on the initial equatorial pitch angle $\alpha_{eq,0}$. We examine whether the trajectory is chaotic by simulating neighboring trajectories with initial velocities rotated by 0.01° and 0.02° of a degree in the azimuthal direction with respect to the original trajectory. We repeat these sets of three simulations while varying M_d and $\alpha_{eq,0}$ and record α_{eq} each time the trajectories intersect the magnetic equator. The results of all simulations appear in Figures S2–S6 in Supporting Information S1 and are summarized in Figure 3c, where each symbol (circles and stars) marks the value of $\alpha_{eq,0}$ and M_d (and for which three simulations of neighboring particles were performed). Chaotic particles lost during the simulation are marked by stars. For particles that remain trapped (circles), the horizontal bars (dotted white lines) show the maximum variation in α_{eq} that they experienced during a simulation (this can be visually inspected in the

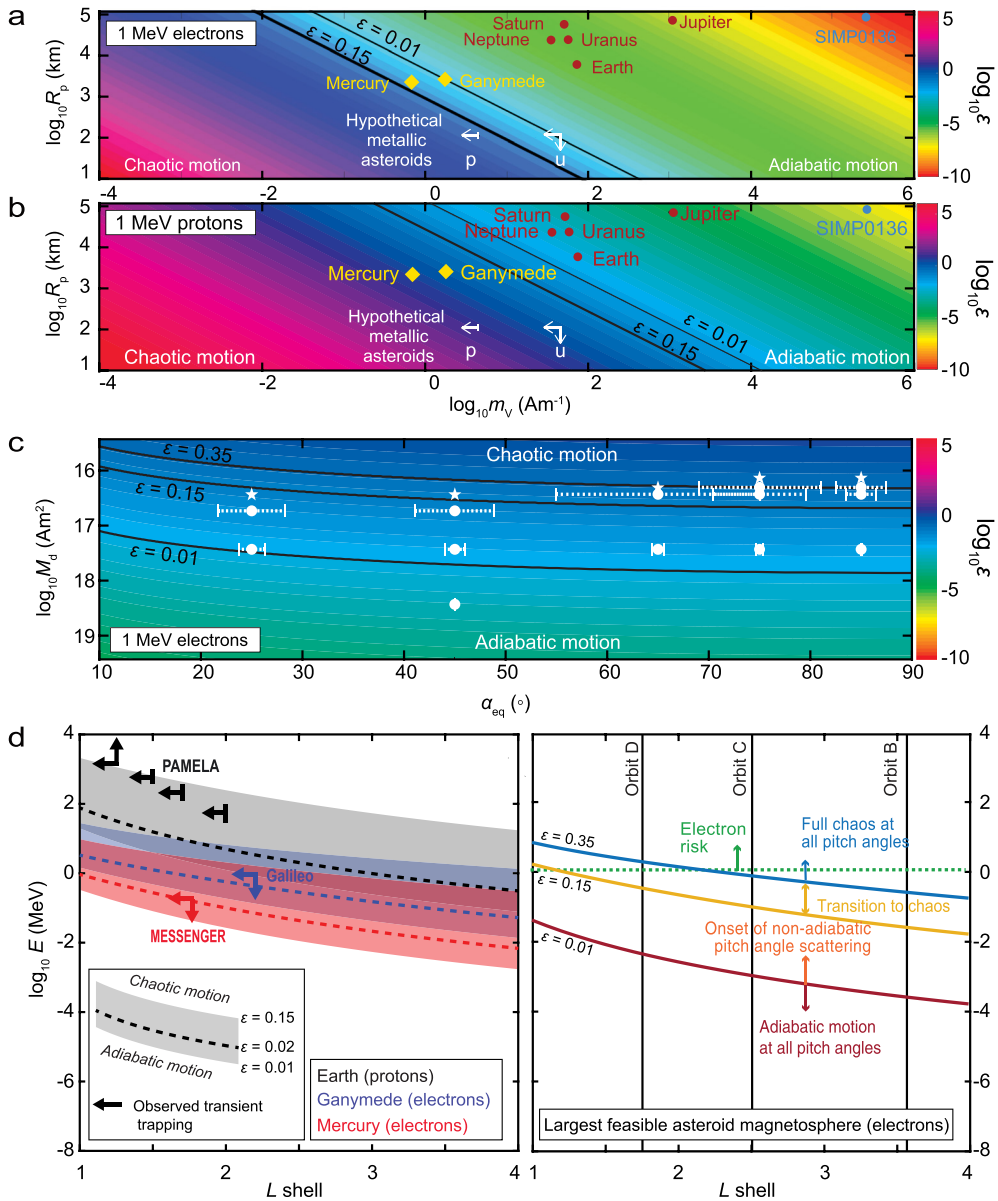

Figure 3. Conditions for trapping protons and electrons around magnetized bodies. (a, b) The adiabaticity parameter, ε, for 1 MeV electrons (a) and protons (b) injected at $L = 2$ with $\alpha_{eq} = 90°$ showing $\varepsilon = 0.15$ (solid black line) and $\varepsilon = 0.01$ (dashed black line). Symbols are as defined in Figure 1a, except for the upper limits for asteroid parameters (white arrows). (c) Adiabatic, nonadiabatic, and chaotic nature of simulated of 1 MeV particles injected at $L = 2$ as a function of equatorial pitch angle, α_{eq} and dipole moment, overlaid on color contours of (in the same color scale as (a)). Chaotic trajectories that end in loss are marked by stars. Trajectories with bounded nonadiabaticity are marked by dotted lines whose lengths represent the span of variations in α_{eq} during the simulation. Circles mark the initial α_{eq}. For fully adiabatic the span of α_{eq} is too small to be visible. (d) Predicted (shaded regions) and observed (arrows) maximum energies of transiently trapped particles versus L. (left) for Earth (protons), Mercury (electrons), and Ganymede (electrons). (right) Electron energies around the largest feasible asteroid magnetosphere for various levels of adiabaticity and chaos. Vertical lines show the altitudes of the Psyche mission science orbits (B, C, and D) (Elkins-Tanton et al., 2020).

corresponding panel in Figures S2–S6 in Supporting Information S1). The values of ε as a function of $\alpha_{eq,0}$ and M_d are plotted for comparison (color contours). We find that for $M_d = 1.35 \times 10^{16}$ Am^2 (50% of the maximum feasible asteroid dipole moment), even particles with $\alpha_{eq,0} = 85°$ become chaotic and are lost almost immediately (Figure S6 in Supporting Information S1). The onset of nonadiabatic motion starts at $\varepsilon = 0.01$ for low $\alpha_{eq,0}$ and full chaos is achieved at $\varepsilon \approx 0.35$ for all $\alpha_{eq,0}$. This value is consistent with the value of $\varepsilon = 0.335$ obtained under

the diffusion approximation for nondipolar magnetic field lines (Young et al., 2008), who solved for the evolution of the entire particle phase-space distribution function. On the other hand, particles with lower $\alpha_{eq,0}$ become chaotic at lower ε, likely because they have higher $v_{\parallel}$ for the same total energy and thus more energy available for resonant interactions between the bounce and gyration motions. This dependence is not captured by ε. The modified adiabaticity parameter, $\varepsilon^* = \varepsilon \cos \alpha_{eq,0}$ (Anderson et al., 1997), does depend on both velocity components, but it would predict that for $\alpha_{eq,0} \approx 80{-}90°$ the motion is adiabatic. In contrast, our simulations show that even large pitch angle particles would experience a transition to chaos in a dipole field with a short length scale. Furthermore, our results are consistent with Cluster measurements that showed depletion of the particle pitch angle distribution for similar ε values near magnetic reconnection topology in Earth's magnetosphere (Zhang et al., 2016).

5. Predictions and Observations of Permanent and Transient Trapping

We apply the ε thresholds established in the previous section to calculate the corresponding maximum energies of trapped populations as a function of L around Ganymede and Mercury (electrons) and at Earth (protons) and compare them to observations (Figure 3d). The Mercury Surface, Space Environment, Geochemistry and Ranging (MESSENGER) spacecraft detected bursts of transiently trapped 100–200 keV electrons at Mercury and no trapped protons (Ho et al., 2011; Lawrence et al., 2015). At Ganymede, the Galileo spacecraft detected trapped <880 keV electrons (Eviatar et al., 2000; Williams, 2001, 2004). Particle simulations (Allioux et al., 2013; Poppe et al., 2018) suggest they likely originated in Jupiter's magnetosphere and only temporarily remained in drift orbits around Ganymede; their high energies do not imply gradual energization of stably trapped particles within Ganymede's magnetosphere, as is typical for radiation belts. Nonetheless, for both Ganymede and Mercury, the observed energies fall well below the energies corresponding to $\varepsilon = 0.15$. This may be due to deviation from a pure dipole field (i.e., the strong day-night asymmetry at Mercury's magnetosphere, Slavin et al., 2007 and the extensive reconnection with Jupiter's magnetic field for Ganymede, Dorelli et al., 2015; Jia et al., 2010; Kivelson, 2007), consistent with our assumption that a static dipole is the worst-case scenario for spacecraft risk.

MESSENGER did not detect trapped protons around Mercury, while Galileo detected <65 keV protons near Ganymede but it was inferred that they moved along open field lines connected to Jupiter (Williams, 2001, 2004; Williams et al., 1997). These findings are consistent with Figure 3b. At Earth, the Payload for Antimatter Exploration and Light-nuclei Astrophysics (PAMELA) detected transiently and permanently trapped protons with energies of 0.2–2 GeV at $L = 1.2{-}2$ (Adriani et al., 2015). The PAMELA observations covered a range of α_{eq}. To make the comparison with Equation 2 consistent, we plot the perpendicular kinetic energy of the detected transiently trapped protons. We find that their maximum energies and L values fall remarkably close to the $\varepsilon = 0.15$ curve at low altitudes while at the highest altitudes the energies are below this curve.

A consistent picture emerges from the particle simulations and observations, allowing us to estimate the maximum electron energies around the largest feasible asteroid magnetosphere (Figure 3e). Permanent trapping becomes increasingly unlikely for $\varepsilon > 0.15$ and essentially impossible for $\varepsilon > 0.35$. At $\varepsilon \approx 0.15$ even particles with $\alpha_{eq,0} > 65°$ experience variations of 5–20° in α_{eq} during the simulations. Any disturbances, such as waves or thermally driven motions could scatter them toward even lower α_{eq} values and push them into the chaotic regime. Calculating the maximum energies for protons (not shown in Figure 3e for clarity) shows that even for $\varepsilon = 0.35$, proton energies do not exceed ~10 keV at $L = 2$, well below risk levels. Nonetheless, low-energy particles may remain trapped.

The threshold of $\varepsilon > 0.15$ corresponds to a maximum gyroradius of approximately:

$$r_g < \frac{r_{eq}}{20} \tag{4}$$

This limit is 5 times smaller than the adiabatic limit. Furthermore, even particles satisfying Equation 4 are not adiabatic and therefore are not guaranteed to remain trapped in a realistic magnetosphere with day-night asymmetries, convective electric fields (which are negligible for asteroids; Section S3 and Figure S1 in Supporting Information S1), reconnection with external fields, and other perturbations. In addition, planetary rings, dusty environments, and neutral particle sources can also absorb or scatter charged particles (Mauk et al., 2004; Nénon & André, 2019; Roussos et al., 2018).

6. Conclusions

We developed a generalized approach for estimating trapped particle energies at any planetary body with a focus on asteroids. Our results have several novel aspects:

1. Combining insights from meteorite paleomagnetism and plasma hybrid modeling in 3D, we showed that asteroid magnetospheres are feasible and obtained an upper limit on their size. However, particle motion in such magnetospheres would be nonadiabatic for particle energies typical of radiation belts.
2. Particle simulations show that chaotic pitch angle scattering limits trapped particle energies for an adiabaticity parameter $\varepsilon \approx 0.15$–0.35 even in the optimal case of a static dipole field. The corresponding particle energies are at least 5 times lower than predicted by adiabatic theory. Such a prediction is consistent with observations of transient trapping at Ganymede, Mercury, and Earth.
3. Even for the strongest feasible dipole moment, asteroids are not likely to permanently trap and >1 MeV electrons and >10 keV protons at $L = 2$ and are unlikely to pose risk to typical space flight systems. However, particles of lower energies may be trapped and form structures like a ring-current system.

Data Availability Statement

The HYB code is distributed under the open source GPL v3 license by the Finnish Meteorological Institute (only available at github: github.com/fmihpc/hyb). Figure data are deposited at figureshare.com, a FAIR-compliant repository (https://doi.org/10.6084/m9.figshare.12957821.v1).

Acknowledgments
This work is supported by the NASA Psyche project (CREI 1576768). Part of the research described in this paper was carried out at the Jet Propulsion Laboratory, California Institute of Technology, under a contract with the National Aeronautics and Space Administration.

References

Adriani, O., Barbarino, G. C., Bazilevskaya, G. A., Bellotti, R., Boezio, M., Bogomolov, E. A., et al. (2015). Trapped proton fluxes at low Earth orbits measured by the PAMELA experiment. *The Astrophysical Journal Letters*, *799*, L4. https://doi.org/10.1088/2041-8205/799/1/l4

Allioux, R., Louarn, P., & André, N. (2013). Model of energetic populations at Ganymede, implications for an orbiter. *Advances in Space Research*, *51*, 1204–1212. https://doi.org/10.1016/j.asr.2012.10.033

Anderson, B. J., Decker, R. B., & Paschalidis, N. P. (1997). Onset of nonadiabatic particle motion in the near-Earth magnetotail. *Journal of Geophysical Research*, *102*, 17553–17569. https://doi.org/10.1029/97JA00798

Baker, D. N., Erickson, P. J., Fennell, J. F., Foster, J. C., Jaynes, A. N., & Verronen, P. T. (2018). Space weather effects in the Earth's radiation belts. *Space Science Reviews*, *214*, 17. https://doi.org/10.1007/s11214-017-0452-7

Berger, M. J., Coursey, J. S., Zucker, M. A., & Chang, J. (2017). *NIST radiation dosimetry database*. NIST. Retrieved from https://www.nist.gov/pml/radiation-dosimetry-data

Birmingham, T. J. (1982). Charged particle motions in the distended magnetospheres of Jupiter and Saturn. *Journal of Geophysical Research*, *87*, 7421–7430. https://doi.org/10.1029/JA087iA09p07421

Blanco-Cano, X., Omidi, N., & Russell, C. T. (2003). Hybrid simulations of solar wind interaction with magnetized asteroids: Comparison with Galileo observations near Gaspra and Ida. *Journal of Geophysical Research*, *108*(A5), 1216. https://doi.org/10.1029/2002JA009618

Carry, B. (2012). Density of asteroids. *Planetary and Space Science*, *73*, 98–118. https://doi.org/10.1016/j.pss.2012.03.009

Chirikov, B. V. (1979). A universal instability of many-dimensional oscillator systems. *Physics Reports*, *53*, 263–379. https://doi.org/10.1016/0370-1573(79)90023-1

Dorelli, J. C., Glocer, A., Collinson, G., & Tóth, G. (2015). The role of the Hall effect in the global structure and dynamics of planetary magnetospheres: Ganymede as a case study. *Journal of Geophysical Research: Space Physics*, *120*, 5377–5392. https://doi.org/10.1002/2014JA020951

Drake, F. D., & Hvatum, S. (1959). Non-thermal microwave radiation from Jupiter. *The Astronomical Journal*, *64*, 329–330. https://doi.org/10.1086/108047

Elkins-Tanton, L. T., Asphaug, E., Bell, J. F., III, Bercovici, H., Bills, B., Binzel, R., et al. (2020). Observations, meteorites, and models: A pre-flight assessment of the composition and formation of (16) Psyche. *Journal of Geophysical Research: Planets*, *125*, e2019JE006296. 10.1029/2019JE006296

Eviatar, A., Williams, D. J., Paranicas, C., McEntire, R. W., Mauk, B. H., & Kivelson, M. G. (2000). Trapped energetic electrons in the magnetosphere of Ganymede. *Journal of Geophysical Research*, *105*, 5547–5554. https://doi.org/10.1029/1999JA900450

Fatemi, S., & Poppe, A. R. (2018). Solar wind plasma interaction with asteroid 16 Psyche: Implication for formation theories. *Geophysical Research Letters*, *45*, 39–48. https://doi.org/10.1002/2017GL073980

Fert, A., & Campbell, I. A. (1976). Electrical resistivity of ferromagnetic nickel and iron based alloys. *Journal of Physics F: Metal Physics*, *6*, 849–871. https://doi.org/10.1088/0305-4608/6/5/025

Gombosi, T. I. (2004). *Physics of the space environment*. Cambridge University Press.

Hales, T. C. (2005). A proof of the Kepler conjecture. *Annals of Mathematics*, *162*, 1065–1185. https://doi.org/10.4007/annals.2005.162.1065

Harrison, R., Bryson, J., Nichols, C., & Weiss, B. (2017). Magnetic mineralogy of meteoritic metal: Paleomagnetic evidence for dynamo activity on differentiated planetesimals. In L. T. Elkins-Tanton, & B. P. Weiss (Eds.), *Planetesimals: Early differentiation and consequences for planets* (pp. 204–223). Cambridge University Press. https://doi.org/10.1017/9781316339794.010

Heslop, D. (2007). Are hydrodynamic shape effects important when modelling the formation of depositional remanent magnetization? *Geophysical Journal International*, *171*, 1029–1035. https://doi.org/10.1111/j.1365-246X.2007.03588.x

Ho, G. C., Krimigis, S. M., Gold, R. E., Baker, D. N., James, A., Anderson, B. J., & Solomon, S. C. (2011). MESSENGER observations of transient bursts of energetic electrons in Mercury's magnetosphere. *Science*, *333*, 1865–1868. https://doi.org/10.1126/science.1211141

Horne, R. B., Thorne, R. M., Glauert, S. A., Albert, J. M., Meredith, N. P., & Anderson, R. R. (2005). Timescale for radiation belt electron acceleration by whistler mode chorus waves. *Journal of Geophysical Research*, *110*, A03225. https://doi.org/10.1029/2004JA010811

Jia, X., Walker, R. J., Kivelson, M. G., Khurana, K. K., & Linker, J. A. (2010). Dynamics of Ganymede's magnetopause: Intermittent reconnection under steady external conditions. *Journal of Geophysical Research*, *115*, A12202. https://doi.org/10.1029/2010JA015771

Kallio, E., & Janhunen, P. (2003). Modelling the solar wind interaction with Mercury by a quasi-neutral hybrid model. *Annales Geophysicae*, *21*, 2133–2145. https://doi.org/10.5194/angeo-21-2133-2003

Kivelson, M. G. (2007). Planetary magnetospheres. In Y. Kamide, & A. Chian (Eds.), *Handbook of the solar-Terrestrial environment* (pp. 469–492). Berlin: Springer-Verlag. https://doi.org/10.1016/b978-012088589-3/50032-3

Kivelson, M. G., Wang, Z., Joy, S., Khurana, K. K., Polanskey, C., Southwood, D. J., & Walker, R. J. (1995). Solar wind interaction with small bodies: 2. What can Galileo's detection of magnetic rotations tell us about Gaspra and Ida. *Advances in Space Research*, *16*, 59–68. https://doi.org/10.1016/0273-1177(95)00209-w

Klida, M. M., & Fritz, T. A. (2009). The Earth's magnetopause as a source and sink for equatorial nightside energetic charged particles. *Annales Geophysicae*, *27*, 4305–4316. https://doi.org/10.5194/angeo-27-4305-2009

Lawrence, D. J., Anderson, B. J., Baker, D. N., Feldman, W. C., Ho, G. C., Korth, H., et al. (2015). Comprehensive survey of energetic electron events in Mercury's magnetosphere with data from the MESSENGER Gamma-Ray and Neutron Spectrometer. *Journal of Geophysical Research: Space Physics*, *120*, 2851–2876. https://doi.org/10.1002/2014JA020792

Lawrence, D. J., Peplowski, P. N., Goldsten, J. O., Burks, M., Beck, A. W., Elkins-Tanton, et al. (2016). The Psyche gamma-ray and neutron spectrometer: Characterizing the composition of a metal-rich body using nuclear spectroscopy. *Paper presented at 47th Lunar and Planetary Science Conference* (abstract #1622), The Woodlands, Texas.

Lee, J. J., Parks, G. K., Min, K. W., McCarthy, M. P., Lee, E. S., Kim, H. J., & Hwang, J. A. (2006). Relativistic electron dropouts by pitch angle scattering in the geomagnetic tail. *Annales Geophysicae*, *24*, 3151–3159. https://doi.org/10.5194/angeo-24-3151-2006

Lemaire, J. F. (2003). The effect of a southward interplanetary magnetic field on Störmer's allowed regions. *Advances in Space Research*, *31*, 1131–1153. https://doi.org/10.1016/S0273-1177(03)00099-1

Li, X., & Liao, S. (2018). Clean numerical simulation: A new strategy to obtain reliable solutions of chaotic dynamic systems. *Applied Mathematics and Mechanics*, *39*, 1529–1546. https://doi.org/10.1007/s10483-018-2383-6

Liuzzo, L., Poppe, A. R., Paranicas, C., Nénon, Q., Fatemi, S., & Simon, S. (2020). Variability in the energetic electron bombardment of Ganymede. *Journal of Geophysical Research: Space Physics*, *125*, e2020JA028347. https://doi.org/10.1029/2020JA028347

Mauk, B. H., & Fox, N. J. (2010). Electron radiation belts of the solar system. *Journal of Geophysical Research*, *115*, A12220. https://doi.org/10.1029/2010JA015660

Mauk, B. H., Mitchell, D. G., McEntire, R. W., Paranicas, C. P., Roelof, E. C., Williams, D. J., et al. (2004). Energetic ion characteristics and neutral gas interactions in Jupiter's magnetosphere. *Journal of Geophysical Research*, *109*, A09S12. https://doi.org/10.1029/2003JA010270

Nénon, Q., & André, N. (2019). Evidence of Europa neutral gas torii from energetic sulfur ion measurements. *Geophysical Research Letters*, *46*, 3599–3606. https://doi.org/10.1029/2019GL082200

Neufeld, J. A., Bryson, J. F. J., & Nimmo, F. (2019). The top-down solidification of iron asteroids driving dynamo evolution. *Journal of Geophysical Research: Planets*, *124*, 1331–1356. 10.1029/2018JE005900

Northrop, T. G. (1963). Adiabatic charged-particle motion. *Reviews of Geophysics*, *1*, 283–304. https://doi.org/10.1029/RG001i003p00283

Pesonen, J. L., Terho, M., & Kukkonen, T. I. (1992). Physical properties of 368 meteorites: Implications of early solar system magnetic fields. In E. M. Zolensky, M. Prinz, & M. Lipschutz (Eds.), *Antarctic meteorites XVII* (pp. 179–181).

Poppe, A. R., Fatemi, S., & Khurana, K. K. (2018). Thermal and energetic ion dynamics in Ganymede's magnetosphere. *Journal of Geophysical Research*, *123*, 4614–4637. https://doi.org/10.1029/2018JA025312

Reeves, G. D., Friedel, R. H., Larsen, B. A., Skoug, R. M., Funsten, H. O., Claudepierre, S., et al. (2016). Energy-dependent dynamics of keV to MeV electrons in the inner zone, outer zone, and slot regions. *Journal of Geophysical Research: Space Physics*, *121*, 397–412. https://doi.org/10.1002/2015JA021569

Richter, I., Brinza, D. E., Cassel, M., Glassmeier, K. H., Kuhnke, F., Musmann, G., et al. (2001). First direct magnetic field measurements of an asteroidal magnetic field: DS1 at Braille. *Geophysical Research Letters*, *28*, 1913–1916. https://doi.org/10.1029/2000GL012679

Roussos, E., Allanson, O., André, N., Bertucci, B., Branduardi-Raymont, G., Clark, G., et al. (2019). *The in-situ exploration of Jupiter's radiation belts (A White Paper submitted in response to ESA's Voyage 2050 Call)*. Arxiv E-prints, arXiv:1908.02339.

Roussos, E., Kollmann, P., Krupp, N., Kotova, A., Regoli, L., Paranicas, C., et al. (2018). A radiation belt of energetic protons located between Saturn and its rings. *Science*, *362*, 6410. https://doi.org/10.1126/science.aat1962

Russell, C. T. (2018). Space and planetary magnetism: From 1958 to the present. In *Sputnik: 60 Years along the path of discoveries* (pp. 143–157). Space Research Institute of the Russian Academy of Sciences.

Scheinberg, A., Fu, R. R., Elkins-Tanton, L. T., Weiss, B. P., & Stanley, S. (2017). Magnetic fields on asteroids and planetesimals. In L. T. Elkins-Tanton, & B. P. Weiss (Eds.), *Planetesimals: Early differentiation and consequences for planets* (pp. 180–203). Cambridge University Press.

Schulz, M., & Lanzerotti, L. J. (1974). Particle diffusion in the radiation belts. In *Physics and chemistry in space* (Vol. 7). Berlin: Springer-Verlag. https://doi.org/10.1007/978-3-642-65675-0

Selesnick, R. S., Cohen, C. M. S., & Khurana, K. K. (2001). Energetic ion dynamics in Jupiter's plasma sheet. *Journal of Geophysical Research*, *106*, 18895–18905. https://doi.org/10.1029/2000JA000242

Serebrennikov, K. S., Gaudin, C., Buzzi, J. M., Bruneteau, J., & Rouille, C. (2001). Non-adiabatic phenomena during magnetic trap confinement and their influence on maximum x-ray energy from electron-cyclotron-resonance-heated plasmas. *Physical Review E*, *63*, 046405. https://doi.org/10.1103/PhysRevE.63.046405

Sergeev, V. A., Sazhina, E. M., Tsyganenko, N. A., Lundblad, J. A., & Soraas, F. (1983). Pitch-angle scattering of energetic protons in the magnetotail current sheet as the dominant source of their isotropic precipitation into the nightside ionosphere. *Planetary and Space Science*, *31*, 1147–1155. https://doi.org/10.1016/0032-0633(83)90103-4

Shepard, M. K., Richardson, J., Taylor, P. A., Rodriguez-Ford, L. A., Conrad, A., dePater, I., & Harris, A. W. (2017). Radar observations and shape model of asteroid 16 Psyche. *Icarus*, *281*, 388–403. https://doi.org/10.1016/j.icarus.2016.08.011

Slavin, J. A., Krimigis, S. M., Acuna, M. H., Anderson, B. J., Baker, D. N., Koehn, P. L., & Zurbuchen, T. H. (2007). Messenger: Exploring Mercury's magnetosphere. *Space Science Reviews*, *131*, 133–160. https://doi.org/10.1007/s11214-007-9154-x

Stern, D. (1971). *Hamiltonian formulation of guiding center motion*(Tech. Rep. NASA-TM-X-65700, X-641-71-373, NASA-TM-X-65458, No. X-641-71-56) NASA Goddard Space Flight Center.

Störmer, C. (1955). *The polar aurora*. Oxford University Press.

Terho, M., Pesonen, L. J., Kukkonen, I. T., & Bukovanska, M. (1993). The petrophysical classification of meteorites. *Studia Geophysica et Geodaetica*, *37*, 65–82. https://doi.org/10.1007/BF01613921

Tsareva, O. O. (2019). Generalization of Störmer theory for an axisymmetric superposition of dipole and quadrupole fields. *Journal of Geophysical Research: Space Physics*, *124*, 2844–2853. https://doi.org/10.1029/2018JA026164
Uckan, N. A. (1982). Temperature limit in ECH hot electron plasmas. *The Physics of Fluids*, *25*, 2381–2384. https://doi.org/10.1063/1.863723
Van Allen, J. A., Ludwig, G. H., Ray, E. C., & McIlwain, C. E. (1958). Observation of high intensity radiation by satellites 1958 Alpha and Gamma (Explorers I and III). *Journal of Jet Propulsion*, *28*, 588–592. https://doi.org/10.2514/8.7396
Voorhies, C. V. (1998). *Elementary theoretical forms for the spatial power spectrum of Earth's crustal magnetic field* (NASA Tech. Pap. 1998-208608, (p. 38).
Voorhies, C. V. (2008). Thickness of the magnetic crust of Mars. *Journal of Geophysical Research*, *113*, E04004. https://doi.org/10.1029/2007JE002928
Voorhies, C. V., Sabaka, T. J., & Purucker, M. (2002). On magnetic spectra of Earth and Mars. *Journal of Geophysical Research*, *107*. https://doi.org/10.1029/2001JE001534
Walsh, B. M., Ryou, A. S., Sibeck, D. G., & Alexeev, I. I. (2013). Energetic particle dynamics in Mercury's magnetosphere. *Journal of Geophysical Research: Space Physics*, *118*, 1992–1999. https://doi.org/10.1002/jgra.50266
Wang, Z., Kivelson, M. G., Joy, S., Khurana, K. K., Polanskey, C., Southwood, D. J., & Walker, R. J. (1995). Solar wind interaction with small bodies: 1. Whistler wing signatures near Galileo's closest approach to Gaspra and Ida. *Advances in Space Research*, *16*, 47–57. https://doi.org/10.1016/0273-1177(95)00208-V
Weiss, B. P., Gattacceca, J., Stanley, S., Rochette, P., & Christensen, U. R. (2010). Paleomagnetic records of meteorites and early planetesimal differentiation. *Space Science Reviews*, *152*, 341–390. https://doi.org/10.1007/s11214-009-9580-z
Wieczorek, M. A. (2018). Strength, depth, and geometry of magnetic sources in the crust of the Moon from localized power spectrum analysis. *Journal of Geophysical Research: Planets*, *123*, 291–316. https://doi.org/10.1002/2017JE005418
Williams, D. J. (2001). Ganymede's ionic radiation belts. *Geophysical Research Letters*, *28*, 3793–3796. https://doi.org/10.1029/2001GL013353
Williams, D. J. (2004). Energetic electron beams in Ganymede's magnetosphere. *Journal of Geophysical Research*, *109*, A09211. https://doi.org/10.1029/2004JA010521
Williams, D. J., Mauk, B., & McEntire, R. W. (1997). Trapped electrons in Ganymede's magnetic field. *Geophysical Research Letters*, *24*, 2953–2956. https://doi.org/10.1029/97GL03003
Young, S. L., Denton, R. E., Anderson, B. J., & Hudson, M. K. (2008). Magnetic field line curvature induced pitch angle diffusion in the inner magnetosphere. *Journal of Geophysical Research*, *113*, A03210. https://doi.org/10.1029/2006JA012133
Zhang, Y. C., Shen, C., Marchaudon, A., Rong, Z. J., Lavraud, B. A., Fazakerley, A., et al. (2016). First in situ evidence of electron pitch angle scattering due to magnetic field line curvature in the Ion diffusion region. *Journal of Geophysical Research: Space Physics*, *121*, 4103–4110. https://doi.org/10.1002/2016ja022409

References From the Supporting Information

Dyadechkin, S., Kallio, E., & Jarvinen, R. (2013). A new 3-D spherical hybrid model for solar wind interaction studies. *Journal of Geophysical Research: Atmospheres*, *118*, 5157–5168. https://doi.org/10.1002/jgra.50497
Ebert, R. W., McComas, D. J., Elliott, H. A., Forsyth, R. J., & Gosling, J. T. (2009). Bulk properties of the slow and fast solar wind and interplanetary coronal mass ejections measured by Ulysses: Three polar orbits of observations. *Journal of Geophysical Research*, *114*, A01109. https://doi.org/10.1029/2008JA013631
Hosea, M. E., & Shampine, L. F. (1996). Analysis and implementation of TR-BDF2. *Applied Numerical Mathematics*, *20*, 21–37. https://doi.org/10.1016/0168-9274(95)00115-8
Kao, M., Hallinan, G., Pineda, J. S., Stevenson, D., & Burgasser, A. (2018). The strongest magnetic fields on the coolest Brown dwarfs. *The Astrophysical Journal—Supplement Series*, *23*(2), 25. https://doi.org/10.3847/1538-4365/aac2d5
Kivelson, M. G., & Russel, C. T. (1995). *Introduction to space physics*. Cambridge University Press.
Lodders, K., & Fegley, B. (1998). *The planetary Scientist's Companion*. Oxford University Press.
McComas, D. J., Barraclough, B. L., Funsten, H. O., Gosling, J. T., Santiago-Munoz, E., Skoug, R. M., et al. (2000). Solar wind observations over Ulysses' first full polar orbit. *Journal of Geophysical Research*, *105*, 10419–10433. https://doi.org/10.1029/1999JA000383
Omidi, N., Blanco-Cano, X., Russell, C. T., Karimabadi, H., & Acuna, M. (2002). Hybrid simulations of solar wind interaction with magnetized asteroids: General characteristics. *Journal of Computational Physics*, *107*, 1487. https://doi.org/10.1029/2002JA009441
Parker, E. N. (1968). Dynamical properties of the magnetosphere. In R. L. Carovillano, J. F. McClay, & H. R. Radoski (Eds.), *Physics of the magnetosphere. Astrophysics and space science library* (Vol. 10). Springer. https://doi.org/10.1007/978-94-010-3467-8_1
Phillips, J. L., Feldman, W. C., Gosling, J. T., & Scime, E. E. (1995). Solar wind plasma electron parameters based on aligned observations by ICE and Ulysses. *Advances in Space Research*, *16*, 95–100. https://doi.org/10.1016/0273-1177(95)00319-A
Russell, C. T., Luhmann, J. G., & Strangeway, R. J. (2016). *Space physics: An introduction*. Cambridge University Press.
Simon, S., Bagdonat, T., Motschmann, U., & Glassmeier, K. H. (2006). Plasma environment of magnetized asteroids: A 3-D hybrid simulation study. *Annales Geophysicae*, *24*, 407–414. https://doi.org/10.5194/angeo-24-407-2006
Tholen, D. J., Tejfel, V. G., & Cox, A. N. (2002). Planets and satellites. In A. N. Cox (Ed.), *Allen's astrophysical quantities* (pp. 293–313). Springer-Verlag. https://doi.org/10.1007/978-1-4612-1186-0_12